Voluntary Swimming Reduces Amyloid Pathology in an Alzheimer's Mouse Brain: An Integrated Amyloid PET/CT and Light-Sheet Microscopy Evaluation

HYE JOO SON[1], SUK HYUN LEE[2], JANG WOO PARK[3], CHANWOO PARK[3], SEONOK KIM[4], SEONGHYUN KIM[5], SOO-JONG KIM[6], YOUNGJAE RYU[7], CHANG MAN HA[7], and CHANWOO KIM[8]

[1]Department of Nuclear Medicine, Dankook University Medical Center, Dankook University College of Medicine, Cheonan, Chungnam, REPUBLIC OF KOREA; [2]Department of Radiology, Hallym University Kangnam Sacred Heart Hospital, Hallym University College of Medicine, Seoul, REPUBLIC OF KOREA; [3]Korea Radioisotope Center for Pharmaceuticals, Korea Institute of Radiological and Medical Sciences, Seoul, REPUBLIC OF KOREA; [4]Department of Clinical Epidemiology and Biostatistics, Asan Medical Center, University of Ulsan College of Medicine, Seoul, REPUBLIC OF KOREA; [5]Dankook Industry Academic Cooperation Foundation, Cheonan, Chungnam, REPUBLIC OF KOREA; [6]Mallinckrodt Institute of Radiology, Washington University School of Medicine in St Louis, Saint Louis, MO; [7]Research Strategy Office and Brain Research Core Facilities of Korea Brain Research Institute (KBRI), Daegu, REPUBLIC OF KOREA; and [8]Department of Nuclear Medicine, Kyung Hee University Hospital at Gangdong, College of Medicine, Kyung Hee University, REPUBLIC OF KOREA

ABSTRACT

SON, H. J., S. H. LEE, J. W. PARK, C. PARK, S. KIM, S. KIM, S.-J. KIM, Y. RYU, C. M. HA, and C. KIM. Voluntary Swimming Reduces Amyloid Pathology in an Alzheimer's Mouse Brain: An Integrated Amyloid PET/CT and Light-Sheet Microscopy Evaluation. *Med. Sci. Sports Exerc.*, Vol. 57, No. 7, pp. 1431–1440, 2025. **Purpose:** Despite numerous observational studies linking exercise to reduced dementia risk, RCT level evidences remain limited to validate physical activity as an effective resistance-augmenting lifestyle intervention. However, transgenic Alzheimer's disease (AD) mouse models circumvent the confounding factors and adherence challenges of human studies by offering rigorous control of exercise regimens, and the capability for advanced three-dimensional imaging to precisely quantify amyloid burden. Using an integrated platform combining [^{18}F]florapronol PET/CT with light-sheet fluorescence microscopy (LSFM) and tissue clearing techniques, we investigated the effect of a 7-wk voluntary swimming on decreasing beta-amyloid (Aβ) pathology in hAPPsw AD mouse. **Methods:** In a prospective interventional study, 20 female AD mice with a mean ± SD age of 63.7 ± 3.4 wk were randomly divided into an intervention and a nonexposure control group (each $n = 10$). A 7-wk voluntary swimming regimen was conducted in 15-cm deep wavy using wave generators, starting with one 10-min session daily during week 1, progressing to six 10-min sessions per day by week 7. The standardized uptake value ratios (SUVRs) were measured using [^{18}F]florapronol PET/CT. The excised brains were then prepared using hydrophilic tissue clearing and volume immunostaining with thioflavin S for Aβ (488 nm). In LSFM imaging, brain Aβ quantitative and morphological parameters were quantified using Imaris-based 3D volumetric surface model. **Results:** In [^{18}F]florapronol PET/CT, swim group exhibited mildly decreased uptake compared with control, although neocortical SUVR differences lacked statistical significance (swim: 1.09 ± 0.14; control: 1.21 ± 0.16, $P = 0.100$). In LSFM imaging, swim group presented significantly lower Aβ accumulation, as indicated by decreases in total surface volume (swim, 76,401,421 ± 14,403,875 μm^3; control, 99,602,785 ± 9,163,020 μm^3; $P < 0.001$) and plaque number (swim, 88,620 ± 15,608; control, 104,612 ± 14,311; $P = 0.007$), than nonexposure control group. There were no statistically significant differences in individual plaque area and volume or in the morphological shape parameters of amyloid particles, such as ellipticity and sphericity. **Conclusions:** We first demonstrated that a 7-wk voluntary swimming is an effective intervention for reducing Aβ pathology in a mouse model of advanced AD. **Key Words:** ALZHEIMER'S DISEASE, AMYLOID, FLORAPRONOL PET/CT, LIGHT-SHEET MICROSCOPE, SWIM

H. J. S., S. H. L, and J. W. P. contributed equally to the manuscript as first authors. Address for correspondence: Hye Joo Son, M.D. Ph.D., Department of Nuclear Medicine, Dankook University Medical Center, Dankook University College of Medicine, Cheonan 31116, Republic of Korea; E-mail: neuroscience@dankook.ac.kr.
Submitted for publication October 2024.
Accepted for publication February 2025.
Supplemental digital content is available for this article. Direct URL citations appear in the printed text and are provided in the HTML and PDF versions of this article on the journal's Web site (www.acsm-msse.org).

0195-9131/25/5707-1431/0
MEDICINE & SCIENCE IN SPORTS & EXERCISE®

DOI: 10.1249/MSS.0000000000003692

Recent challenges with monoclonal antibody therapies for Alzheimer's disease (AD), including high costs and side effects such as cerebral hemorrhage, have shifted attention to lifestyle-based prevention strategies (1). In parallel, the concept of resistance has gained prominence, referring to individuals who exhibit lower-than-expected levels of pathology despite risk factors for AD (2). According to the 2020 dementia report by the Lancet Commission, improving twelve modifiable lifestyle factors could reduce the incidence of dementia worldwide by 40% (3). Among various modifiable lifestyle interventions, physical activity is particularly crucial, as it can reduce the global prevalence of dementia by 2%, potentially translating into substantial cost savings—an estimated

US$40 billion out of the projected US$2 trillion in dementia care costs (4,5).

Numerous observational studies link leisure-time physical activities with a reduced dementia risk in nondemented elderly individuals. For example, in a large Finnish prospective study, midlife leisure-time physical activity at least twice a week was linked to a 50% lower risk of dementia (6). Greater daily walking distances were associated with reduced dementia risk in retired Japanese-American men in the Honolulu-Asia Aging Study (7). However, variability in study populations, protocols (exercise items, frequency, duration), and assessment methods limits generalizability, and evidence from randomized controlled trials (RCTs) remains insufficient. Notably, the LIFE trial showed no significant cognitive benefits in a general elderly population, with effects observed only in subgroup analyses of individuals over 80 yr old or with low baseline activity (8). Additionally, according to the 2018 American Health and Human Services Physical Activity Guidelines, the protective effect of exercise on cognition has been demonstrated in individuals aged 6–13 yr and those over 50, but its effect on dementia prevention in young to middle-aged adults (18–50 yr) remains unproven (9). Therefore, these knowledge gaps highlight the need for well-designed interventional studies to establish causality and refine exercise-based prevention strategies.

Investigating the preventive effects of exercise on dementia requires the precision and control offered by transgenic AD mouse models, which overcome the inherent limitations of human studies. Minimizing confounding factors—including comorbidities, lifestyle, and genetic heterogeneity—in human research is challenging. Additionally, human observational studies often depend on retrospective self-reporting, and even randomized trials face challenges with participant adherence, thus limiting the precise quantification of exercise interventions as intended by researchers. To address these constraints, we employed a transgenic AD mouse model featuring a uniform genetic background and tightly controlled housing conditions, allowing researchers to isolate exercise as the principal independent variable and enable precise manipulation and standardization of exercise frequency, intensity, and duration, resulting in more reliable assessments of its impact on pathology. Furthermore, our study prioritizes the reduction of amyloid pathology—rather than clinical symptoms—as the primary outcome to determine whether exercise effectively alters early biological processes before cognitive deficits emerge. By employing a transgenic AD mouse model, we were able to use advanced tissue clearing techniques and light-sheet fluorescence microscopy (LSFM) to visualize the entire transparent brain in three dimensions, enabling precise quantification of total amyloid burden and the morphological properties of individual aggregates, thus facilitating a more comprehensive analysis of preventive interventions. Among various exercise items, we selected voluntary swimming, a moderate-intensity regimen that can be systematically adjusted in duration, interval, frequency, and consistency. This method offers advantages in terms of human translatability and permitted a more physiological intervention than forced swimming or treadmill running with electric shocks, which may introduce stress-related confounders.

In this prospective animal interventional study, using an integrated imaging platform that combines [^{18}F]florapronol PET/CT with LSFM and tissue clearing techniques, we aimed to elucidate the effect of a 7-wk voluntary swim exercise regimen on decreasing amyloid pathology in a transgenic mouse model of AD.

METHODS

Animal model. The study included 20 female C57BL/6-Tg(NSE-hAPPsw)Korl transgenic mice, commonly referred to as the hAPPsw model, with a mean ± SD age of 63.7 ± 3.4 wk at the time of experimentation, which express hAPP with the Swedish mutation under the control of NSE promoter. The transgenic line was originally developed to model aspects of AD pathology, specifically the overproduction of beta-amyloid (Aβ) peptides. All mice were housed in a temperature-controlled environment (22°C ± 2°C, 55% ± 10% relative humidity) with a 12-h light/12-h dark cycle, given *ad libitum* access to standard rodent feed and water, and accommodated in standard polycarbonate cages with autoclaved wood shavings and enrichment materials. The mice were given a 1-wk acclimatization period before any experimental procedures. All animal experiments were conducted in conformance with the policy statement of the American College of Sports Medicine on research with experimental animals and approved by the Dankook Institutional Animal Care and Use Committee and conducted in accordance with their guidelines and regulations (DKU-23-041).

Voluntary swimming exercise regimen. The swimming exercise, on the basis of previous research (10,11), was conducted using a stainless-steel water tank (Φ900 × H450 mm/550 mm) filled with fresh warm water at a controlled temperature (32°C ± 1°C) and equipped with three identical wave generators arranged in an equilateral triangle to ensure that the mice were compelled to swim and unable to merely float (see Supplemental Video 1, Supplemental Digital Content 1). Twenty transgenic AD mice were randomly divided into two subgroups: voluntary swim (n = 10) and nonexposure control (n = 10). The exercise regimen involved swimming 5 d·wk^{-1} for 7 wk, with each session consisting of a 10-min swim followed by a 10-min rest. During the first week, the mice were acclimated to a shallow water depth (5 cm) for daily 10-min sessions. From the second to third week, the water depth was increased to 15 cm, and the swimming duration was extended to 20 min·d^{-1} (two 10-min sessions). In the fourth to fifth weeks, the swimming duration was increased to 30 min daily (three 10-min sessions). By the sixth to seventh weeks, the swimming duration was increased to 60 min·d^{-1} (six 10-min sessions). After each exercise session, the mice in the intervention group were carefully removed from the tank, dried with paper towels, and kept warm with an infrared lamp during the 10-min rest session. The nonexposure control group was placed in a same empty water tank and allowed free movement for the same time duration.

Amyloid PET/CT acquisition. PET/CT imaging was performed using a nanoScan PET/CT system (Mediso, Hungary). All mice were anesthetized (2.5%–3.0% isoflurane in 100% O_2 gas) and received an intravenous injection of [^{18}F]florapronol (Alzavue®) (200 μCi/200 μL) through the tail vein for PET/CT

imaging. After a 30-min uptake period following [^{18}F]florapronol administration, static PET images were acquired for 30 min with an energy level of 400–600 keV, a 5-ns coincidence time window, and 1:5 coincidence mode. CT imaging was then performed for both anatomical reference and attenuation correction with the following parameters: 50 kVp, 580 μA, 170 ms exposure time, 1:4 binning, and 250 × 250 × 250 μm voxel size. PET images were reconstructed using Tera-Tomo 3D in full detector mode with regularization and 4 × 6 iterations × subsets, resulting in a voxel size of 0.4 mm.

PET/MR imaging processing. In order to analyze amyloid uptake on [^{18}F]florapronol imaging between the voluntary swim group and the control group, we conducted PET-only quantitative analysis using an in-house amyloid-specific mouse brain PET template for spatial normalization without MRI for the mouse models. This template was constructed using data from an independent group of nine control mice that underwent both amyloid PET and 7 T MRI scans. Initially, PET images from these nine control mice were coregistered to their corresponding 7-T MRI images using PMOD software (version 3.4, PMOD Technologies Ltd., Zurich, Switzerland). Because the mouse T2 template embedded in PMOD was skull stripped, we manually performed skull stripping on the control mice using ITK-SNAP to create brain masks on individual T2 MR images. These masks were then applied to the MRI and spatially normalized to the mouse brain T2 template (12,13). The coregistered PET images were normalized to the template space using MRI normalization parameters, and a final template was generated by averaging and smoothing these normalized images.

In both the swim group and the control group, spatial normalization was performed by cropping the whole-body PET scans to preserve only the head region and to align the scans with the mouse brain PET template. These head-region images were first aligned to our in-house mouse brain PET template using rigid body registration and then spatially normalized to the template space. Finally, the mouse atlas in PMOD was used for ROI-based quantitative analysis of the spatially normalized PET images (14).

Hydrophilic clearing process and volume immunostaining for Aβ in brain samples. In accordance with protocols established by the Institutional Animal Care and Use Committee, mice were euthanized using isoflurane anesthesia. Specifically, each mouse was placed in an induction chamber filled with 5% isoflurane mixed with oxygen. To effectively remove blood from the whole-brain vasculature, transcardial perfusion with 1× phosphate-buffered saline (PBS) was conducted on mice that were deeply anesthetized but still alive. Subsequently, the brain tissues were then fixed with a 4% paraformaldehyde (PFA) solution in PBS. After fixation, the brains were dissected and subjected to overnight postfixation at 4°C in 4% PFA. A 1-mm sagittal section was then dissected, specifically targeting the CA1 hippocampal region, with coordinates relative to the bregma: −2 mm anterior/posterior, ±1.8 mm lateral/medial, and −1.5 mm dorsal/ventral. Tissue clearing was achieved using a hydrophilic Binaree Tissue Clearing Kit (HRTI-012; Binaree, Daegu, Korea). PFA was removed by three washes with 1× PBS at 4°C, each lasting 20 min. The samples were then submerged in 10 mL of starting solution and incubated at 37°C for 48 h while shaking at 50 rpm. The solution in each tube was then replaced with 10 mL of tissue clearing solution A, and the incubation was repeated. Each tube was rinsed four times with distilled water at 4°C, each wash lasting 30 min. The solution was then substituted with 3 mL of tissue clearing solution B, and the samples were incubated again at 37°C for 12 h while shaking at 50 rpm. To visualize Aβ plaques, the samples were treated with thioflavin S, which emits at 488 nm. The plaques were stained with a 1% thioflavin S solution in 50% ethanol, incubated at 25°C, shaken at 50 rpm for 15 min, and then washed three times with 1× PBS at 4°C, each wash lasting 20 min. Finally, the samples were incubated in 6 mL of mounting and storage solution (SHMS-060, Binaree) at 37°C for 48 h while shaking at 50 rpm to match the high refractive index of the tissue and render the tissues transparent. Mounted samples were stored in the dark at room temperature until LSFM.

LSFM imaging acquisition and Imaris software-based automated quantitative analysis of 3D volumetric surface model generation. LSFM imaging was performed using a Lightsheet Z.1 microscope system (Carl Zeiss Meditec, Inc., Oberkochen, Germany). LSFM was supported by Brain Research Core Facilities in KBRI. The illumination lens, a 5× (Carl Zeiss, 0.1 NA) at air and a 5× objective lens (Carl Zeiss, EC Plan-Neofluar, 0.16 NA), with a 0.71× zoom factor was used for optical image acquisition. The excitation source was a $\lambda = 488$ nm laser (30 mW, Diode laser; Lasos Laser GmbH, Germany) for the detection of cerebral Aβ deposition. The data were acquired by sCMOS camera (1920 × 1920 pixel resolution, PCO.Edge; Excelitas Technologies, Pittsburgh, PA). Our cleared brain slice samples achieved a sufficient signal-to-noise ratio with single side illumination mode, which assisted to reduce phototoxicity. All acquisitions were controlled by the ZEN software (version 9.2.7.54, Carl Zeiss). Czi files by ZEN were converted into an Ims file format by Imaris converter, and the stitching was performed using the Imaris stitcher (version 9.2.1, Bitplane). Quantitative image evaluation was performed using Imaris software (version 9.2.1; Bitplane AG, Zurich, Switzerland). The dimensions of the three-dimensional volumetric data (length, width, and height) were each downscaled to 25% of their original size to optimize computational efficiency during image analysis. For the 488-nm laser wavelength utilized for Aβ detection, an automated computational surface model was generated using the Surface Creation Wizard embedded in the Imaris software environment. The minimal discernible feature size for Aβ detection was set at 4.0 μm, corresponding to the smallest detected diameter of the targeted Aβ particle within the slice-mode observations. Local contrast enhancement mode was applied for background subtraction to segregate the true signal from extraneous noise. An automated thresholding approach defined the largest permissible feature size in the extraneous background, which was then manually refined to ensure that the constructed surfaces accurately replicated the morphological attributes of the cellular markers while minimizing aberrant noise. Statistical validation was conducted by applying a 95% confidence interval to the voxel dimensions, accurately determining the volumetric characteristics of the surface models. Volumetric data extraction was facilitated through the "Statistics" functionality within the "Surpass" tab of the Imaris interface, with the "Volume" metric specifically selected from the available measurement parameters.

Statistical analysis. Data normality was assessed using the Shapiro–Wilk test. Variables that met the normality assumption were analyzed using the *t*-test and are presented as mean ± SD. nonnormally distributed (skewed) variables were analyzed using the Wilcoxon rank-sum test and are reported as medians with interquartile ranges (median [IQR]). Longitudinal changes in body weight over a 7-wk period between the voluntary swim group and the nonexposure control group were assessed using random coefficients model with restricted cubic splines (15). This model included fixed effects for time, group, and the interaction between time and group and individual-specific random effects for intercept and slope. Differences in weight change between the swim group and the control group at three time points—baseline (day 0), mid-intervention (day 19), and postintervention (day 38)—were further assessed using *t*-tests. Weight changes from baseline to day 19 and from baseline to day 38 between groups were evaluated to determine statistical significance. A two-sided *P* value less than 0.05 was considered statistically significant. All statistical analyses were performed using SAS version 9.4 (SAS Institute; Cary, NC) and R version 4.2.2 (R Foundation for Statistical Computing) with lme4 and rms package.

RESULTS

Effect of the exercise intervention on body weight change. The longitudinal trend of daily weight measurements over 7 wk in the voluntary swim group and the nonexposure control group was identified using random coefficients model (Supplemental Fig. 1, Supplemental Digital Content 4, http://links.lww.com/MSS/D199). Both groups exhibited an initial decrease in weight from the start of the swim sessions until mid-intervention (day 19), followed by an increase from mid-intervention to the end of the sessions. Although there was no significant difference in the time trends of weight change between the two groups (NumDF = 4, DenDF = 123.25, *F* value = 2.38, *p* for interaction = 0.056), the voluntary swim group showed a significantly greater weight decrease from baseline to day 19 compared with the control group (voluntary swim group: mean = −3.69 ± 1.53; nonexposure control: mean = −2.10 ± 1.80; *P* = 0.047). Overall, the total weight change from baseline to the day 38 end point of the intervention showed that the voluntary swim group gained significantly less weight than the control group (voluntary swim group: mean = 0.67 ± 1.62 kg; control group: mean = 3.03 ± 1.80 kg; *P* = 0.006).

Effect of voluntary swimming on [^{18}F]florapronol PET/CT imaging. In the visual analysis of [^{18}F]florapronol brain PET/CT imaging (Fig. 1), the voluntary swim group exhibited mildly decreased Aβ uptake compared with the nonexposure control group. In the quantitative analysis of subregional SUVR using cerebellar gray matter as the reference region (Fig. 2 and Table 1), the voluntary swim group showed

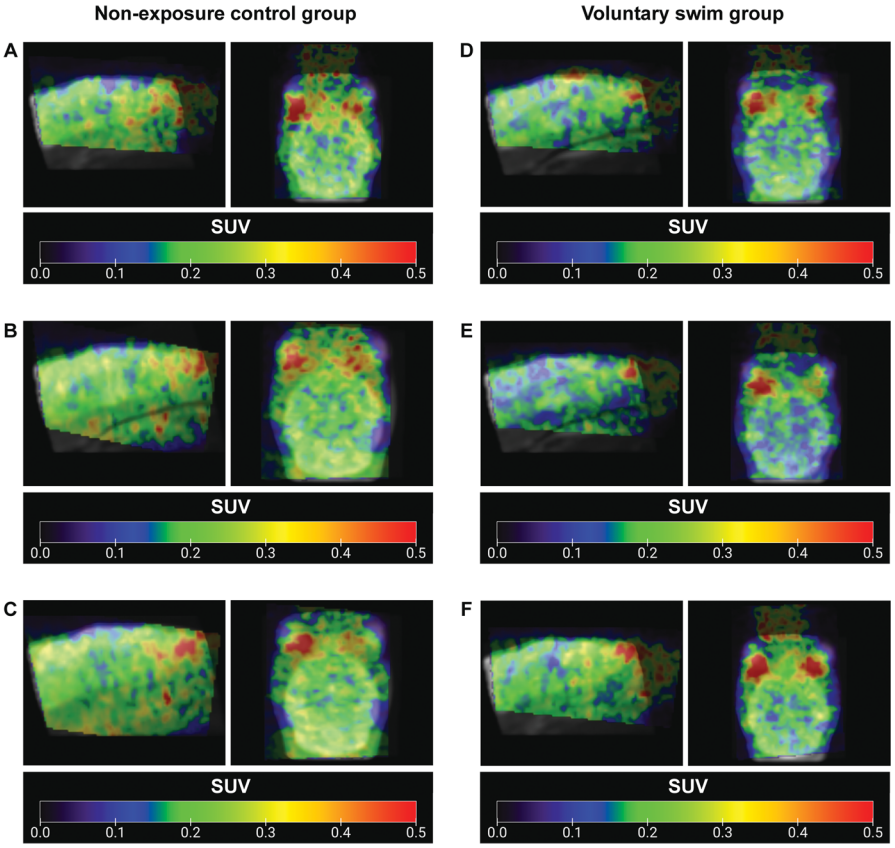

FIGURE 1—Representative [^{18}F]florapronol PET/CT images. A, B, C. The nonexposure control group. D, E, F. The voluntary swim group. Note: the color bar represents the SUV scale from 0 to 0.5.

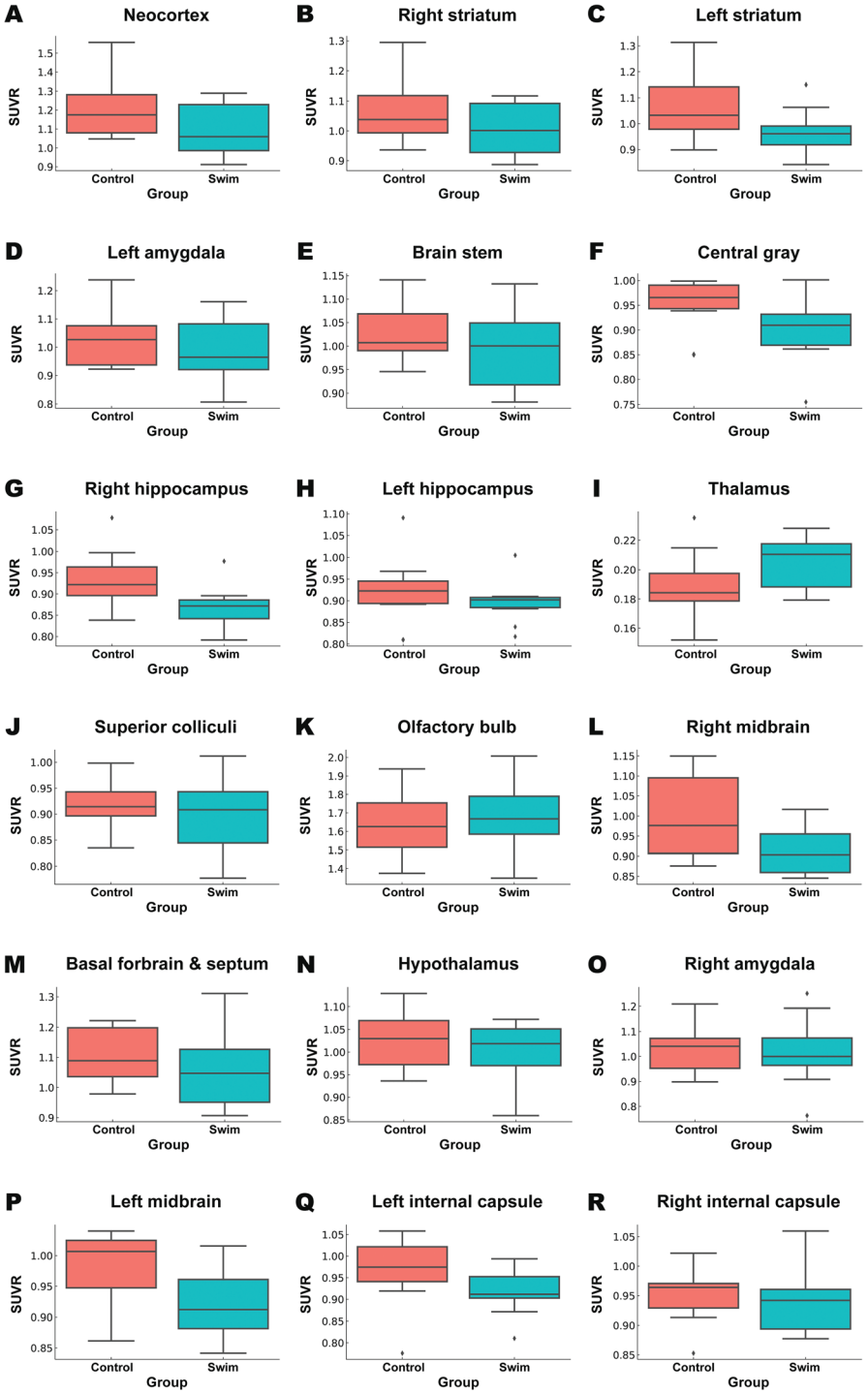

FIGURE 2—Comparison of SUVR values in [^{18}F]flurapronol PET/CT images between the voluntary swim group (n = 10) and the nonexposure control group (n = 10) across various brain subregions (A, neocortex; B, right striatum; C, left striatum; D, left amygdala; E, brain stem; F, central gray; G, right hippocampus; H, left hippocampus; I, thalamus; J, superior colliculi; K, olfactory bulb; L, right midbrain; M, basal forebrain and septum; N, hypothalamus; O, right amygdala; P, left midbrain; Q, left internal capsule; R, right internal capsule).

mildly lower mean SUVR in the neocortex, bilateral striatum, bilateral hippocampus, hypothalamus, bilateral amygdala, brainstem, central gray, superior colliculi, and left midbrain regions compared with the control group. However, these differences in SUVR values were not statistically significant (neocortex: voluntary swim group: mean = 1.09 ± 0.14; nonexposure control: mean = 1.21 ± 0.16; P = 0.100).

Effect of voluntary swimming on the total Aβ load and 3D morphological features in brain LSFM imaging. Using an advanced LSFM and hydrophilic tissue clearing chemical techniques, we conducted a comprehensive investigation into the three-dimensional spatial distribution of Aβ accumulation, labeled with thioflavin S (488 nm, green channel), in the brains of the voluntary swim group and the nonexposure control group. In

TABLE 1. Comparison of subregional SUVR values of [^{18}F]florapronol PET/CT imaging between the voluntary swim group and the nonexposure control group.

Brain Subregion	Voluntary Swim Group (n = 10)	Nonexposure Control Group (n = 10)	P
Neocortex	1.09 ± 0.14	1.21 ± 0.16	0.100
Right striatum	1.00 ± 0.09	1.07 ± 0.13	0.176
Left striatum	0.97 ± 0.09	1.07 ± 0.13	0.006
Right hippocampus	0.87 ± 0.05	0.94 ± 0.07	0.024
Left hippocampus	0.90 ± 0.05	0.92 ± 0.08	0.445
Thalamus	0.20 ± 0.02	0.19 ± 0.02	0.126
Basal forebrain and septum	1.06 ± 0.13	1.10 ± 0.09	0.429
Hypothalamus	1.00 ± 0.07	1.03 ± 0.07	0.391
Right amygdala	1.02 ± 0.14	1.04 ± 0.11	0.770
Left amygdala	0.99 ± 0.12	1.03 ± 0.10	0.466
Brain stem	0.99 ± 0.09	1.03 ± 0.06	0.335
Central gray	0.97 (0.94–0.99)	0.91 (0.87–0.93)	0.162
Superior colliculi	0.90 ± 0.08	0.92 ± 0.05	0.440
Olfactory bulb	1.68 ± 0.19	1.64 ± 0.18	0.599
Right midbrain	0.91 ± 0.06	1.00 ± 0.10	0.039
Left midbrain	0.92 ± 0.06	0.98 ± 0.06	0.026
Left internal capsule	0.92 ± 0.05	0.97 ± 0.08	0.117
Right internal capsule	0.95 ± 0.06	0.95 ± 0.05	0.849

Data are presented as mean ± SD for normally distributed variables, or as median (IQR) for nonnormally distributed variables.
* $P < 0.05$ is considered statistically significant.

both groups, Aβ accumulation was predominantly distributed throughout the whole-brain cortex, particularly in the bilateral temporal, parietal, frontal, and anterior cingulate cortex, as well as in the hippocampus and thalamus. A visual comparison between the voluntary swim group and the nonexposure control group revealed that the mice subjected to 7 wk of voluntary swim training presented significantly lower Aβ accumulation than the control mice did (Fig. 3 and Supplemental Video 2, Supplemental Digital Content 2, and Supplemental Video 3, Supplemental Digital Content 3). For our quantitative analysis via Imaris software, we generated 3D volumetric surface models to measure various parameters of brain Aβ plaques, including the individual plaque size (individual plaque area and volume), variability in individual plaque size (SD of individual plaque volume), total plaque load (total plaque number, surface area, and volume), and morphological shape parameters (individual plaque ellipticity [both oblate and prolate] and sphericity) (Table 2 and Fig. 4). The total surface volume of Aβ accumulation in the brains of the voluntary swim group was significantly lower than that of the nonexposure control group (voluntary swim group, 76.40 ± 14.40 mm^3; nonexposure control, 99.60 ± 9.16 mm^3; $P < 0.001$). This difference remained significant in a linear regression analysis adjusted for weight change ($P < 0.003$). The total surface area of Aβ accumulation in the brains of the voluntary swim group was also significantly lower than that of the nonexposure control group (voluntary swim group, 35.85 ± 9.88 mm^2; nonexposure control, 46.28 ± 4.30 mm^2; $P = 0.010$). This difference also remained significant in a linear regression analysis adjusted for weight change ($P < 0.029$). The total plaque number was also significantly lower in the voluntary swim group than in the nonexposure control group, (voluntary swim group, 88619.60 ± 15607.99; nonexposure control, 104,613 ± 14,311; $P = 0.007$). However, there were no statistically significant differences between the groups in terms of the individual plaque area (voluntary swim group, 405 ± 54 μm^2; nonexposure control, 447 ± 55 μm^2; $P = 0.186$) or individual plaque volume (voluntary swim group, 771 ± 143 μm^3; nonexposure control, 906 ± 183 μm^3; $P = 0.162$). The variability in the individual plaque size, measured by the SD of the individual plaque volume, did not differ significantly between the groups (voluntary swim group, 1,772 ± 335 μm^3; nonexposure control, 2,333 ± 966 μm^3; $P = 0.104$). Additionally, there were no statistically significant differences in the morphological shape parameters of individual amyloid particles, such as ellipticity (oblate: voluntary swim group, 0.15 ± 0.01; nonexposure control, 0.16 ± 0.00; P = 0.076),

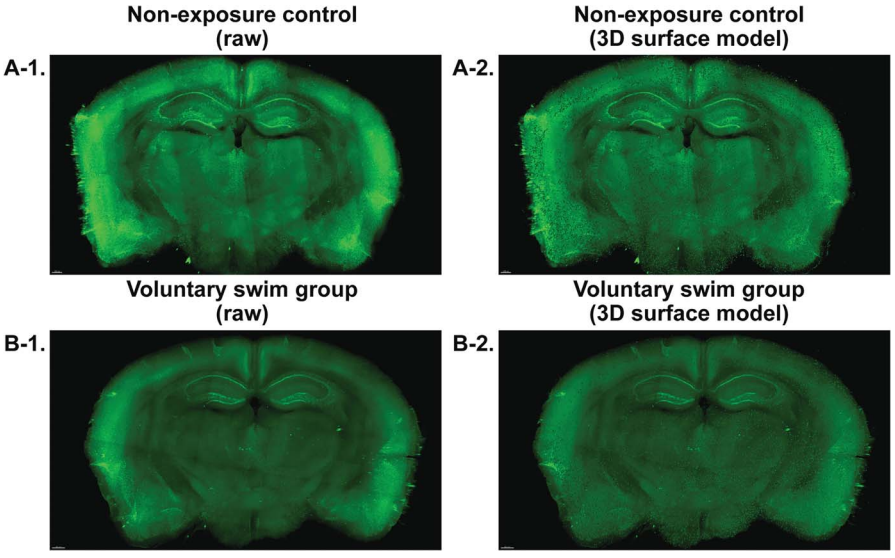

FIGURE 3—Representative macrolaser light-sheet illuminating microscope image with hydrophilic tissue clearing and volume immunostaining using thioflavin S (488 nm, *green channel*) for Aβ in the brain. A. The nonexposure control group: A-1, raw image; A-2, Imaris-based volume rendering surface model. B. The voluntary swim group: B-1, raw image; B-2, Imaris-based volume rendering surface model.

TABLE 2. Comparison of quantitative and morphological parameters of brain amyloid measure using macrolaser LSFM imaging between the voluntary swim group and the nonexposure control group.

Volume	Voluntary Swim Group (n = 10)	Nonexposure Control Group (n = 10)	P*	P**
Individual plaque area (μm^2)	405.48 (358.50–447.27)	432.0855 (426.113–441.337)	0.186	
Individual plaque volume (μm^3)	771.89 (637.05–882.97)	857.533 (828.041–885.789)	0.162	
SD of individual plaque volume (μm^3)	1760.89 (1501.31–1886.41)	2039.43 (1810.48–2182.68)	0.104	
Total plaque number	92836.5 (83121–98285)	102551.5 (101516–110862)	0.007*	
Total plaque surface area (μm^2)	35,851,640 ± 9,883,776	46,282,448 ± 4,300,066	0.010*	0.029**
Total plaque surface volume (μm^3)	76,401,421 ± 14,403,875	99,602,785 ± 9,163,020	<0.001*	0.003**
Ellipticity (oblate)	0.15 ± 0.01	0.16 ± 0.00	0.076	
Ellipticity (prolate)	0.78 ± 0.01	0.78 ± 0.01	0.081	
Sphericity	0.71 (0.70–0.71)	0.70 (0.70–0.71)	0.820	

Data are presented as mean ± SD for normally distributed variables, or as median (IQR) for nonnormally distributed variables.
* P < 0.05 is considered statistically significant for t-tests or Wilcoxon rank-sum tests.
** P < 0.05 is considered statistically significant for linear regression analyses adjusted for weight change.

ellipticity (prolate: voluntary swim group, 0.78 ± 0.01; nonexposure control, 0.78 ± 0.01; P = 0.081), or sphericity (voluntary swim group, 0.70 ± 0.01; nonexposure control, 0.71 ± 0.00; P = 0.820).

DISCUSSION

Our integrated imaging platform, combining [^{18}F]florapronol PET/CT with LSFM, revealed that the voluntary swim exercise group exhibited reduced amyloid accumulation, as measured by total amyloid surface volume, compared with nonexposure controls. Although derived from a mouse model, these findings indicate that leisure-time voluntary swimming may help mitigate amyloid pathology—even in advanced stages of AD.

Evidence indicates that aerobic exercise promotes brain function and cognition across the lifespan through a range of molecular and cellular mechanisms—particularly those supporting endothelial integrity, improving sleep, and reducing pathological protein aggregates (16–20). Various factors that could influence our results include the age and sex of the animals; the environmental conditions under which the swimming took place, such as the water depth, temperature, and wave intensity; the duration of daily swimming; the intervals between swimming and rest periods; and the overall duration of the swimming regimen. We selected voluntary swimming in wavy water generated by wave machines as our choice of intervention, as this protocol does not cause significant pain or intense stress to the animals and maintains physiological stability during the intervention sessions. Forced and voluntary exercise differentially influence hippocampal parvalbumin and BDNF expression, longevity, body composition, taste aversion learning, and open-field behavior (21–26) due to high stress levels, reduced brain BDNF expression, and impaired motor recovery (21). In an ischemic stroke rat model, voluntary wheel running was more effective than forced treadmill running or electrical stimulation–induced muscle movement in increasing hippocampal BDNF levels, enhancing motor recovery, and reducing corticosterone stress responses (21). Forced exercise, associated with high stress, lower BDNF expression, and impaired motor recovery, appears to be the least favorable option (21). Forced swimming also may further elevate blood lactate concentrations due to apnea and stress from the risk of drowning (27). Furthermore, voluntary swimming, a moderate-intensity exercise, has shown the strongest preventive effect against dementia onset by increasing resistance to AD pathology (28). In the cognitively healthy late- to middle-aged Wisconsin Registry cohort, it was associated with higher Aβ42 levels and lower total tau/Aβ42 and phosphorylated tau/Aβ42 ratios compared with light- or high-intensity exercise (28). We adapted our swimming protocol from previous studies on voluntary swimming programs (10,11,29). In 11- to 12-wk-old rats with type 2 diabetes, a 4-wk voluntary swimming regimen (up to 60 min·d^{-1}) reduced depression-like behavior by mitigating inflammation (10). Long-term exercise from adolescence to adulthood, incorporating voluntary wheel running, swimming (up to 60 min·d^{-1}), or treadmill exercise on alternating days for 3 months, significantly reduced anxiety and depression-like behaviors in offspring (11). Given differences in weight, basal metabolic rate, and neurobiological circuits between transgenic AD mice and nondemented rats—as well as the advanced age and heightened sensitivity to novel stimuli in our 63-wk-old model—we modified the swimming protocol from previous studies to extend

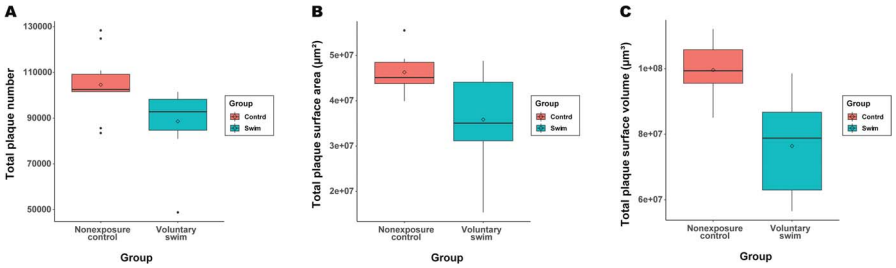

FIGURE 4—Comparison of the total Aβ load and 3D morphological features in the brain LSFM images between the voluntary swim group (n = 10) and the nonexposure control group (n = 10). Total plaque number (A), total plaque surface area (μm^2) (B), total plaque surface volume (μm^3) (C).

the total duration to 7 wk, with daily sessions of up to 60 min, aiming to balance stress prevention and health maintenance with the maximal efficacy of exercise on AD pathology.

To evaluate the effects of a 7-wk voluntary swimming regimen on reducing amyloid pathology in a transgenic AD mouse model, we used an integrated imaging platform combining [^{18}F]florapronol amyloid PET/CT with LSFM and tissue clearing techniques. In our study, we used [^{18}F]florapronol as the in vivo amyloid PET/CT imaging tracer (30). Compared with other [^{18}F]-labeled Aβ PET tracers approved by the FDA, such as [^{18}F]flutemetamol (45–130 min) (31) and [^{18}F] florbetaben (90 min) (32), [^{18}F]florapronol offers the clinical advantage of a shorter waiting time of approximately 30 min between tracer administration and the start of PET imaging (33). However, although visual analysis of [^{18}F]florapronol PET/CT images showed mildly reduced amyloid uptake in the voluntary swim group compared with controls, the difference in neocortical SUVRs was not statistically significant. Although amyloid PET imaging is invaluable for the noninvasive early detection of amyloid pathology in AD patients (34,35), translating this technique to preclinical mouse studies presents significant challenges. The small size of the mouse brain, approximately 1/1,000 the volume of the human brain, amplifies the inherent limitations of small-animal PET imaging, leading to partial volume effects that blur or underestimate amyloid plaque signals. This reduced resolution complicates the precise quantification of amyloid distribution in specific brain regions. Moreover, current semiquantitative methods using SUVR cannot reliably distinguish between specific binding of radiotracers to Aβ and nonspecific binding to other targets, particularly β-sheet structured myelin protein in white matter (36,37). The cortical gray matter regions used for amyloid quantification also contain myelinated axons, resulting in the integration of nonspecific signals into SUVR estimates (37). The low spatial resolution of small-animal PET scanners further exacerbates this issue, causing white matter signals to spill into gray matter regions, reducing imaging sensitivity and resolution, complicating the precise quantification of subtle pathological changes (36,37). Therefore, LSFM used in our study provides a complementary solution to the spatial resolution limitations of conventional amyloid PET imaging in preclinical research. It offers a broad field of view without compromising spatial resolution, enabling whole-brain imaging while preserving 3D integrity. This approach provides comprehensive insights into the 3D spatial distribution of complex neuropathological networks within the fully transparent brain, a capability previously unattainable with conventional techniques (38–41). Building on previous animal studies of exercise and brain pathology, this study not only quantifies the total amyloid load but also provides detailed measurements of individual plaque area, volume, variability in individual plaque volume, and morphological features. These parameters were difficult to assess with traditional techniques, which relied on spot counting in thin 2D sections of localized subregions, limiting the ability to evaluate the 3D spatial distribution of Aβ within intact brain structures.

Our analysis first demonstrated that 63-wk-old transgenic AD mice subjected to a 7-wk voluntary swimming regimen (up to 60 min daily in 15 cm deep, wavy water) had reduced Aβ accumulation, as measured by total amyloid surface volume, compared with nonexposure controls. This difference of total surface volume between swim and control groups remained significant in a linear regression analysis adjusted for weight change ($P < 0.003$), suggesting that the observed reduction in Aβ accumulation was not solely attributable to changes in body weight and may reflect an independent effect of exercise on amyloid pathology. Our decision to use total surface volume—calculated by summing the 3D rendered surface volumes of individual amyloid plaques using Imaris software—as a representative measure of an individual's overall amyloid load is based on the premise that volumetric measurements offer a more accurate reflection of the true extent of pathological amyloid burden than simply counting the number of plaques (42). In addition to significantly reducing total amyloid surface volume, the voluntary swim exercise regimen decreased the overall surface area and total plaque number without affecting the area or volume of individual plaques, suggesting that the voluntary swim regimen reduced the net amyloid load in the brain primarily by decreasing the number of amyloid particles rather than by altering the size or shape of existing plaques. Moreover, morphological features such as ellipticity and sphericity remained unchanged. By integrating total amyloid load assessment with detailed morphological analysis of individual plaques, our platform overcomes the limitations of conventional amyloid PET imaging, enabling a more comprehensive evaluation of preventive interventions in AD pathology.

Despite the promising findings, several limitations should be noted. First, the sample size was small (10 mice per group), which may have contributed to the lack of statistical differences in [^{18}F]florapronol PET SUVR between the groups and could limit the generalizability of the results. Second, the 7-wk intervention may not have been sufficient to assess the long-term effects of voluntary swimming on amyloid pathology. Third, although LSFM provided detailed insights into amyloid plaque distribution and morphology, it does not capture functional aspects of neuroprotection or cognitive outcomes. Most importantly, from a human translational perspective, the use of a transgenic AD mouse model may not fully capture the complexity of human sporadic dementia. Future studies with larger cohorts, extended intervention periods, and functional assessments are needed to further validate and expand these findings.

In conclusion, using an advanced integrated imaging platform that integrates [^{18}F]florapronol PET/CT with LSFM and hydrophilic tissue clearing techniques, we demonstrate that voluntary swimming reduces amyloid pathology in a mouse model of advanced AD. Further research is needed to assess the translatability of these findings to humans.

The present study was funded by FutureChem Co., Ltd, and supported by the National Research Foundation of Korea (NRF) grant funded by the Ministry of Science and ICT (MIST), Republic of Korea (grant number 2021R1F1A1063874; PI: Hye Joo Son), the KBRI research program through Korea Brain Research Institute funded by the Ministry of Science, ICT & Future Planning (grant number 24-BR-03-02; PI: Chang

Man Ha), and the grant of the Korea Institute of Radiological and Medical Sciences (KIRAMS), funded by Ministry of Science and ICT(MSIT), Republic of Korea (grant number 50539-2024, PI: Yong Jin Lee).

This study was conducted at the Lab of Tissue Clearing Imaging and Behavior of Alzheimer's Brain, directed by the corresponding author and principal investigator, Prof. Hye Joo Son, at Dankook University College of Medicine. The authors acknowledge the Division of RI Application, the Korea Institute of Radiological and Medical (KIRAMS) for their assistance with [18F]florapronol PET/CT imaging. They also thank brain research core facilities in the Korea Brain Research Institute (KBRI) for their support in acquiring LSFM imaging acquisition. They are grateful to the department of Clinical Epidemiology and Biostatistics at Asan Medical Center for their support in statistical analysis. Special thanks to Dr. Soo-Jong Kim from the Mallinckrodt Institute of Radiology, Washington University School of Medicine in St. Louis, for his assistance with PET/MR image processing and quantitative analysis. Finally, the authors extend their profound gratitude to Prof. Suk Hyun Lee, who leads the artificial intelligence imaging research laboratory at the Department of Radiology, Hallym University Kangnam Sacred Heart Hospital, for his support in data interpretation and visualization.

Conflicts of interest and source of funding: Hye Joo Son received research grants from FutureChem Co., Ltd. The other authors declare no conflicts of interest, financial or otherwise. The results of the study are presented clearly, honestly, and without fabrication, falsification, or inappropriate data manipulation. The results of the present study do not constitute endorsement by the American College of Sports Medicine.

Statement of human and animal rights: The animal study protocol was approved by the Dankook Institutional Animal Care and Use Committee, adhering to the respective guidelines and regulations (DKU-23-041).

Data availability statement: All data generated or analyzed during this study are included in this published article (and its supplementary information files).

REFERENCES

1. Park KW. Anti-amyloid antibody therapies for Alzheimer's disease. *Nucl Med Mol Imaging*. 2024;58(4):227–36.
2. Arenaza-Urquijo EM, Vemuri P. Resistance vs resilience to Alzheimer disease: clarifying terminology for preclinical studies. *Neurology*. 2018;90(15):695–703.
3. Livingston G, Huntley J, Sommerlad A, et al. Dementia prevention, intervention, and care: 2020 report of the lancet commission. *Lancet*. 2020;396(10248):413–46.
4. World Health Organization. *Global Action Plan on the Public Health Response to Dementia 2017–2025*. World Health Organization; 2017.
5. Prince M, Wimo A, Guerchet M, et al. *World Alzheimer Report 2015. The Global Impact of Dementia: An Analysis of Prevalence, Incidence, Cost and Trends*. Alzheimer's Disease International; 2015.
6. Rovio S, Kareholt I, Helkala EL, et al. Leisure-time physical activity at midlife and the risk of dementia and Alzheimer's disease. *Lancet Neurol*. 2005;4(11):705–11.
7. Abbott RD, White LR, Ross GW, et al. Walking and dementia in physically capable elderly men. *JAMA*. 2004;292(12):1447–53.
8. Sink KM, Espeland MA, Castro CM, et al. Effect of a 24-month physical activity intervention vs health education on cognitive outcomes in sedentary older adults: the LIFE randomized trial. *JAMA*. 2015;314(8):781–90.
9. Erickson KI, Hillman C, Stillman CM, et al. Physical activity, cognition, and brain outcomes: a review of the 2018 physical activity guidelines. *Med Sci Sports Exerc*. 2019;51(6):1242–51.
10. Gilak-Dalasm M, Peeri M, Azarbayjani MA. Swimming exercise decreases depression-like behaviour and inflammatory cytokines in a mouse model of type 2 diabetes. *Exp Physiol*. 2021;106(9):1981–91.
11. Rahimi S, Peeri M, Azarbayjani MA, et al. Long-term exercise from adolescence to adulthood reduces anxiety- and depression-like behaviors following maternal immune activation in offspring. *Physiol Behav*. 2020;226:113130.
12. Yushkevich PA, Yang G, Gerig G. ITK-SNAP: an interactive tool for semi-automatic segmentation of multi-modality biomedical images. *Annu Int Conf IEEE Eng Med Biol Soc*. 2016;2016:3342–5.
13. Mirrione MM, Schiffer WK, Fowler JS, Alexoff DL, Dewey SL, Tsirka SE. A novel approach for imaging brain-behavior relationships in mice reveals unexpected metabolic patterns during seizures in the absence of tissue plasminogen activator. *Neuroimage*. 2007;38(1):34–42.
14. Ma Y, Hof PR, Grant SC, et al. A three-dimensional digital atlas database of the adult C57BL/6J mouse brain by magnetic resonance microscopy. *Neuroscience*. 2005;135(4):1203–15.
15. Brown H, Prescott R. *Applied Mixed Models in Medicine*. UK: John Wiley & Sons; 2014.
16. Trigiani LJ, Hamel E. An endothelial link between the benefits of physical exercise in dementia. *J Cereb Blood Flow Metab*. 2017;37(8):2649–64.
17. Tarasoff-Conway JM, Carare RO, Osorio RS, et al. Clearance systems in the brain-implications for Alzheimer disease. *Nat Rev Neurol*. 2015;11(8):457–70.
18. Medeiros R, LaFerla FM. Astrocytes: conductors of the Alzheimer disease neuroinflammatory symphony. *Exp Neurol*. 2013;239:133–8.
19. Ide K, Secher NH. Cerebral blood flow and metabolism during exercise. *Prog Neurobiol*. 2000;61(4):397–414.
20. Stillman CM, Esteban-Cornejo I, Brown B, Bender CM, Erickson KI. Effects of exercise on brain and cognition across age groups and health states. *Trends Neurosci*. 2020;43(7):533–43.
21. Arida RM, Scorza CA, da Silva AV, Scorza FA, Cavalheiro EA. Differential effects of spontaneous versus forced exercise in rats on the staining of parvalbumin-positive neurons in the hippocampal formation. *Neurosci Lett*. 2004;364(3):135–8.
22. Ke Z, Yip SP, Li L, Zheng XX, Tong KY. The effects of voluntary, involuntary, and forced exercises on brain-derived neurotrophic factor and motor function recovery: a rat brain ischemia model. *PLoS One*. 2011;6(2):e16643.
23. Ploughman M, Granter-Button S, Chernenko G, Tucker BA, Mearow KM, Corbett D. Endurance exercise regimens induce differential effects on brain-derived neurotrophic factor, synapsin-I and insulin-like growth factor I after focal ischemia. *Neuroscience*. 2005;136(4):991–1001.
24. Narath E, Skalicky M, Viidik A. Voluntary and forced exercise influence the survival and body composition of ageing male rats differently. *Exp Gerontol*. 2001;36(10):1699–711.
25. Masaki T, Nakajima S. Taste aversion in rats induced by forced swimming, voluntary running, forced running, and lithium chloride injection treatments. *Physiol Behav*. 2006;88(4–5):411–6.
26. Burghardt PR, Fulk LJ, Hand GA, Wilson MA. The effects of chronic treadmill and wheel running on behavior in rats. *Brain Res*. 2004;1019(1–2):84–96.
27. Dos Reis IGM, Martins LEB, de Araujo GG, Gobatto CA. Forced swim reliability for exercise testing in rats by a tethered swimming apparatus. *Front Physiol*. 2018;9:1839.
28. Law LL, Rol RN, Schultz SA, et al. Moderate intensity physical activity associates with CSF biomarkers in a cohort at risk for Alzheimer's disease. *Alzheimers Dement (Amst)*. 2018;10:188–95.
29. Bashiri H, Enayati M, Bashiri A, Salari AA. Swimming exercise improves cognitive and behavioral disorders in male NMRI mice with sporadic Alzheimer-like disease. *Physiol Behav*. 2020;223:113003.
30. Lee BS, Chu SY, Kwon HR, et al. Synthesis and evaluation of 6-(3-[(18)F]fluoro-2-hydroxypropyl)-substituted 2-pyridylbenzothiophenes and 2-pyridylbenzothiazoles as potential PET tracers for imaging Aβ plaques. *Bioorg Med Chem*. 2016;24(9):2043–52.
31. Vandenberghe R, Van Laere K, Ivanoiu A, et al. 18F-flutemetamol amyloid imaging in Alzheimer disease and mild cognitive impairment: a phase 2 trial. *Ann Neurol*. 2010;68(3):319–29.
32. Barthel H, Gertz HJ, Dresel S, et al. Cerebral amyloid-β PET with florbetaben (18F) in patients with Alzheimer's disease and healthy

controls: a multicentre phase 2 diagnostic study. *Lancet Neurol*. 2011; 10(5):424–35.
33. Byun BH, Kim BI, Park SY, et al. Head-to-head comparison of 11C-PiB and 18F-FC119S for Aβ imaging in healthy subjects, mild cognitive impairment patients, and Alzheimer's disease patients. *Medicine (Baltimore)*. 2017;96(12):e6441.
34. Kim JS, Son HJ, Oh M, Lee DY, Kim HW, Oh J. 60 years of achievements by KSNM in neuroimaging research. *Nucl Med Mol Imaging*. 2022;56(1):3–16.
35. Bom HH, Kim J, Yun M, Kang DY. Are the nuclear neuro-imaging biomarkers reliable? *Nucl Med Mol Imaging*. 2024;58(4):158–9.
36. Heurling K, Buckley C, Vandenberghe R, Laere KV, Lubberink M. Separation of β-amyloid binding and white matter uptake of (18)F-flutemetamol using spectral analysis. *Am J Nucl Med Mol Imaging*. 2015;5(5):515–26.
37. Liu H, Nai Y-H, Chen C, Reilhac A. *Deep learning-based estimation of non-specific uptake in amyloid-PET images from structural MRI for improved quantification of amyloid load in Alzheimer's disease. In: Proceedings of the 2020 IEEE 33rd International Symposium on Computer-Based Medical Systems (CBMS)*. Rochester (MN); 2020 Jul 28–30. pp. 573–8.
38. Keller PJ. Imaging morphogenesis: technological advances and biological insights. *Science*. 2013;340(6137):1234168.
39. Krzic U, Gunther S, Saunders TE, Streichan SJ, Hufnagel L. Multiview light-sheet microscope for rapid in toto imaging. *Nat Methods*. 2012;9(7):730–3.
40. Mertz J. Optical sectioning microscopy with planar or structured illumination. *Nat Methods*. 2011;8(10):811–9.
41. Truong TV, Supatto W, Koos DS, Choi JM, Fraser SE. Deep and fast live imaging with two-photon scanned light-sheet microscopy. *Nat Methods*. 2011;8(9):757–60.
42. Crassin C. GigaVoxels: a voxel-based rendering pipeline for efficient exploration of large and detailed scenes. *HAL Theses*. 2011;2011: 1–207.